New techniques for reconstructing and calibrating hadronic objects with ATLAS

Matthew Green

On behalf of the ATLAS Collaboration

ML4Jets 2026, 14th-18th of September, Vienna

Outline

- Many physics measurements/searches are driven by hadronic objects
  - Making sure that these hadronic objects are well reconstructed and calibrated is high priority for ATLAS
- ML serves as the perfect tool to improve hadronic understanding

This talk gives a taste of the most recent ML developments within the ATLAS collaboration surrounding hadronic reconstruction & calibration

Hadronic Objects

- Jets represent the hadronic showers in the detector
- Built via the anti-k_T algorithm with radius parameter R, where:
  - Small-R (R = 0.4) represent quark/gluons
  - Large-R (R=1.0) represent boosted topologies (W,Z, H, t)
- Different constituents can be used to form jets:
  - "EMTopo" – uses calorimeter-only information to construct topological clusters (topo-clusters)
  - "Particle-Flow" – includes a combined measurement from the entire detector
- Machine learning can be used at both the constituent-level, as well as a jet-level

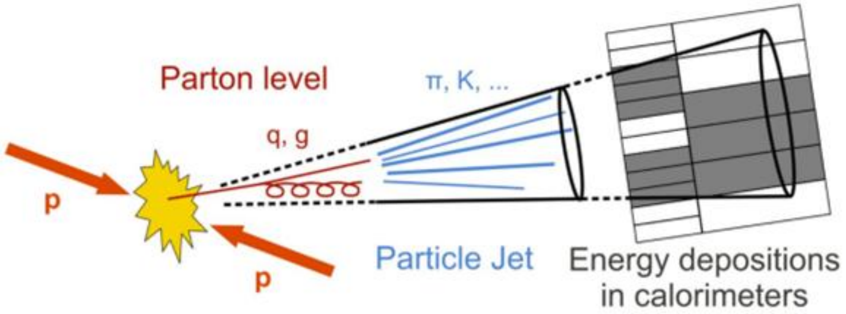

Precision calibration of calorimeter signals in the ATLAS experiment using an uncertainty-aware neural network

JETM-2024-01 & JETM-2026-04

NN-based topo-cluster calibration

- The goal of the calibration is to recover the deposited $\mathrm{E}_{clus}^{\mathrm{truth}}$ of clusters within jets
  - Training target: $R_{clus}^{\mathrm{EM}} = \frac{\mathrm{E}_{clus}^{\mathrm{EM}}}{\mathrm{E}_{clus}^{\mathrm{truth}}} = \frac{\mathrm{reco}}{\mathrm{truth}}$
- Inputs: Cluster-Level observables, χ_{clus}

$$\{\underbrace{E_{\mathrm{clus}}^{\mathrm{EM}}, y_{\mathrm{clus}}^{\mathrm{EM}}}_{\text{kinematics}}, \overbrace{\zeta_{\mathrm{clus}}^{\mathrm{EM}}}^{\text{signal relevance}}, \underbrace{\mathrm{Var}_{\mathrm{clus}}(t_{\mathrm{cell}}), \lambda_{\mathrm{clus}}, |\vec{c}_{\mathrm{clus}}|, \langle\rho_{\mathrm{cell}}\rangle, \langle \mathfrak{m}_{\mathrm{long}}^2\rangle, \langle \mathfrak{m}_{\mathrm{lat}}^2\rangle, p_{\mathrm{T}}D, f_{\mathrm{emc}}}_{\text{shower nature (position, compactness, signal density and internal time structure)}}, \overbrace{f_{\mathrm{iso}}}^{\text{topology (isolation)}}, \underbrace{t_{\mathrm{clus}}, N_{\mathrm{PV}}, \mu}_{\text{pile-up}}\}$$

- Data: All clusters in jets from QCD Dijets

Bayesian Neural Network (BNN)

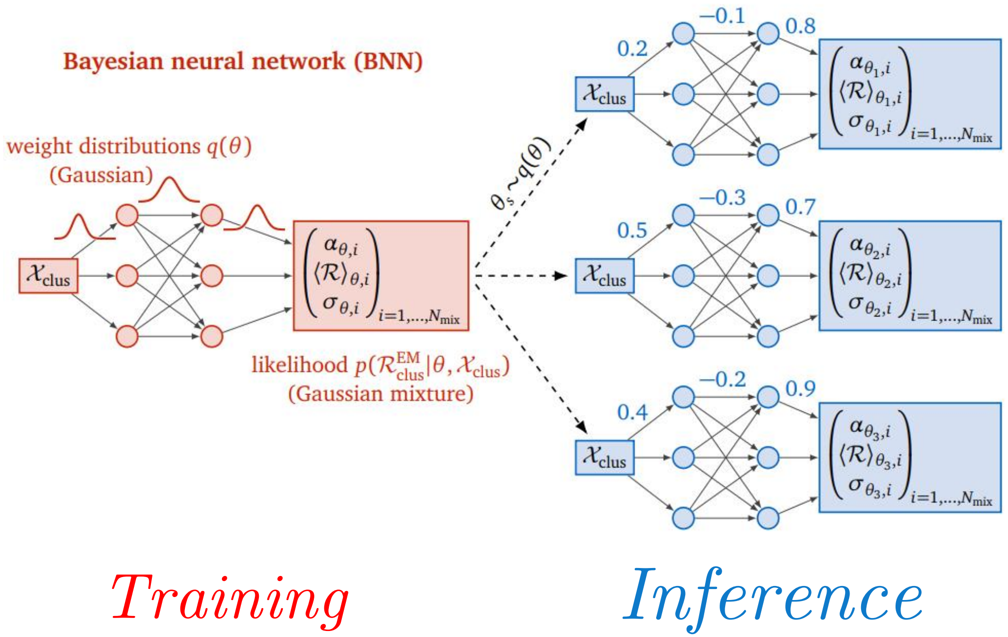

$$p\left(\left\{R^{\mathrm{EM}}_{\mathrm{clus}}\right\}|\theta,\{\chi_{\mathrm{clus}}\}\right)=\sum_{i=1}^{N_{mix}}\alpha_{\theta,i}\mathcal{N}\left(R^{\mathrm{EM}}_{\mathrm{clus}}\,|R_{\theta,i}\,,\sigma_{\theta,i}\right)$$

- Unlike traditional NNs, BNNs use weight distributions, $q(\theta)$
- During inference, the network is sampled multiple times to produce an average predicted likelihood
  - 3-component Gaussian Mixture where:
    - $\alpha_{\theta,i}$ - mixture weight
    - $R_{\theta,i}$ - the predicted value
    - $\sigma_{\theta,i}$ - standard deviation
- Therefore, the BNN provides most probable response, as well as an estimation of uncertainty
  - Hence, “uncertainty-aware” network

DNN-HGM

- Deployment of a BNN had served to be difficult
- Replacement:
  Heteroscedastic Gaussian Mixture (HGM)
  - Simulates the BNN by using a Gaussian Mixture output head
  - Learns to predict the Gaussian Mixture parameters by minimising the heteroscedastic loss
  - Deterministic due to the fixed weights
  - Much easier to implement for inference
- Still produces prediction of a PDF per cluster than can be used for calibration

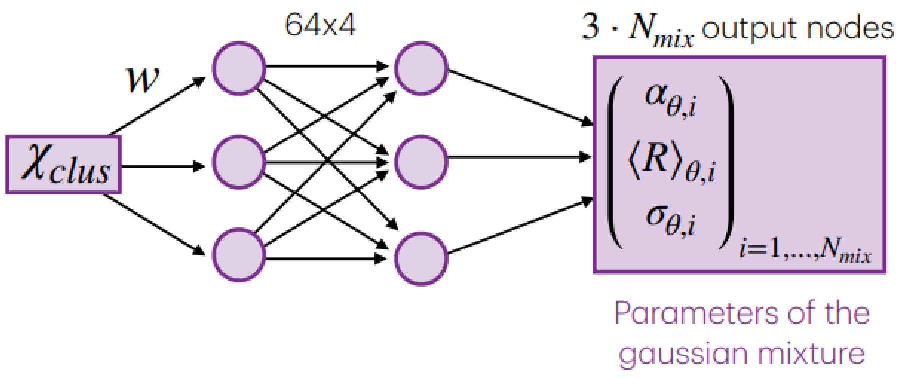

$$p\left(\left\{R_{\text{clus}}^{\text{EM}}\right\} | \theta, \{\chi_{\text{clus}}\}\right) = \sum_{i=1}^{N_{mix}} \alpha_{\theta,i} \mathcal{N}\left(R_{\text{clus}}^{\text{EM}} | R_{\theta_i}, \sigma_{\theta_i}\right)$$

<u>Same output as BNN!</u>

Performance

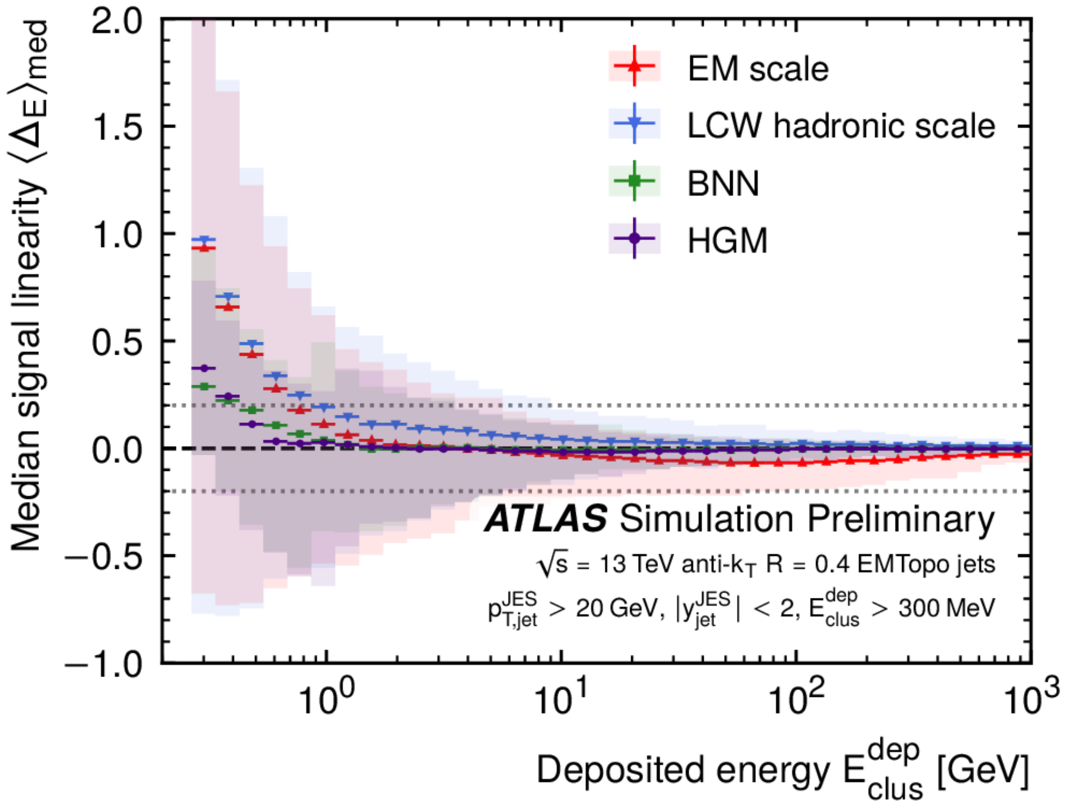

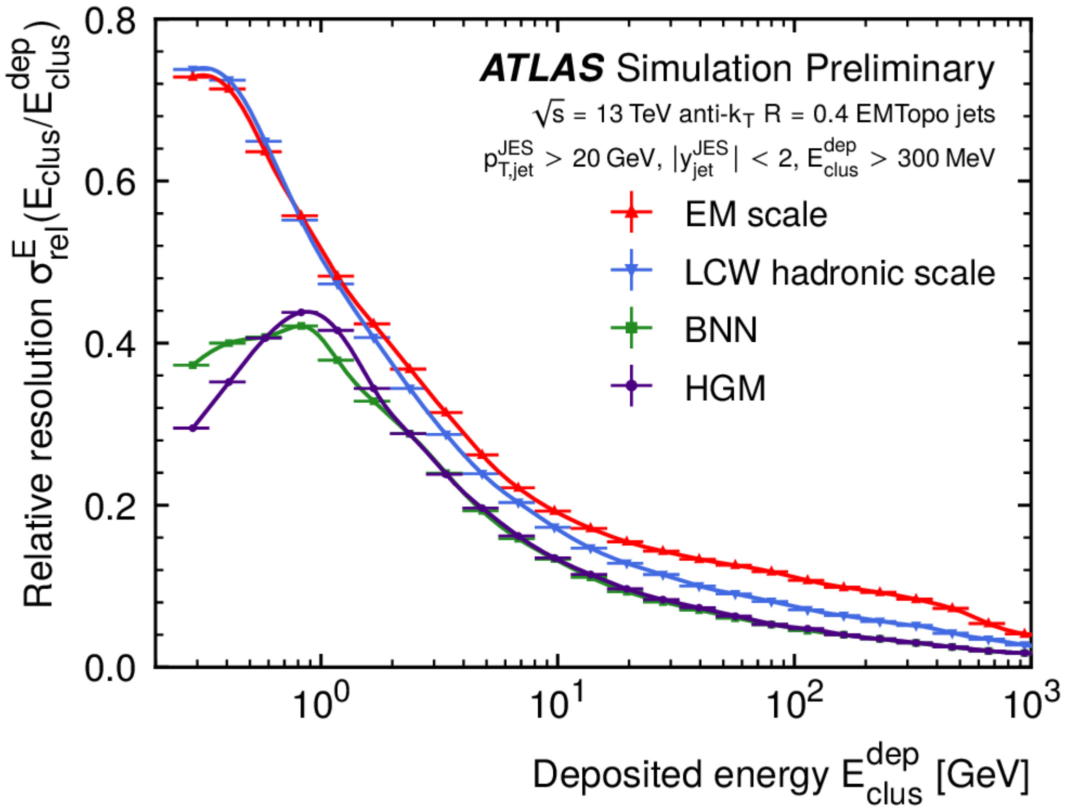

- Both the BNN & HGM outperform the two baselines
  - HGM is much less complicated implementation to get similar results.

Performance in PU-conditions

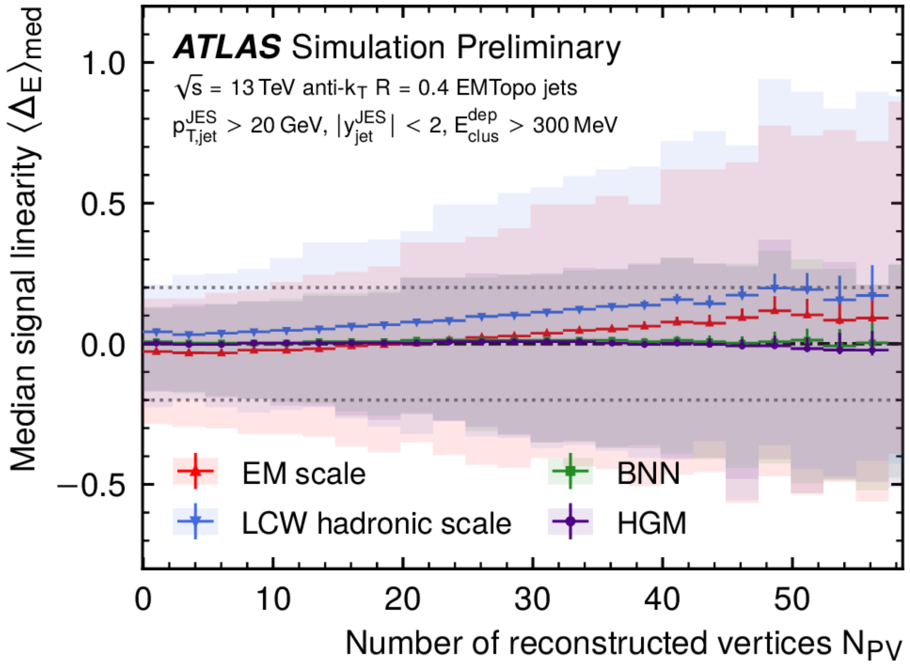

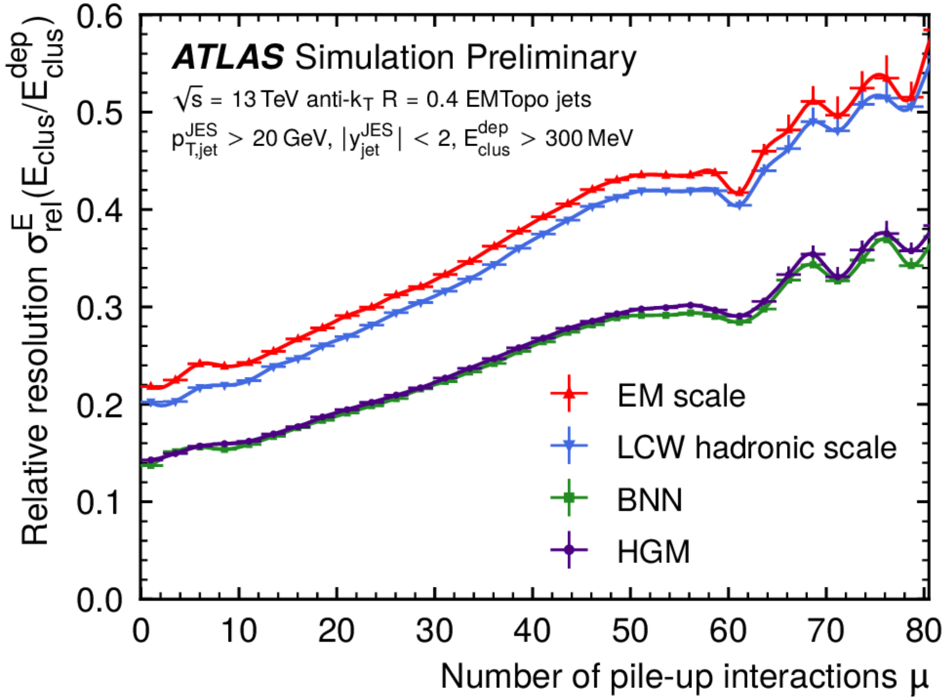

- Since the input includes PU-related variables, it is able to learn the pile-up dependence of the calibration
  - BNN/HGM again outperforms the baseline over the entire range of N_{PV} / μ
  - Important feature leading into the HL-LHC era

Jet calibration

- ATLAS uses a multi-step jet calibration chain, each correcting different aspects of the reconstruction
  - Goal: Recover the truth jet-scale at particle-level
- Integration of advanced ML-based calibration to supplement (or replace) the traditional jet calibration chain requires careful study
  - Especially important thinking towards HL-LHC era
- Two figures of merit:
  - Jet-Energy-Scale (JES): mean of the gaussian
  - Jet-Energy-Resolution (JER): width of the gaussian

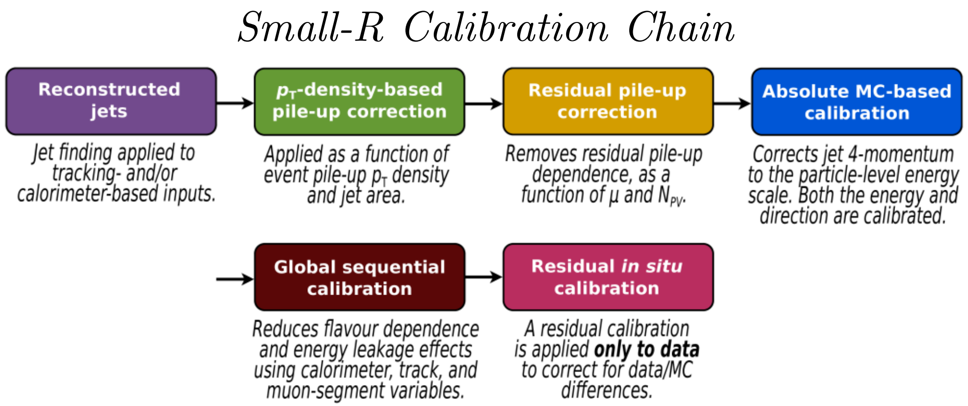

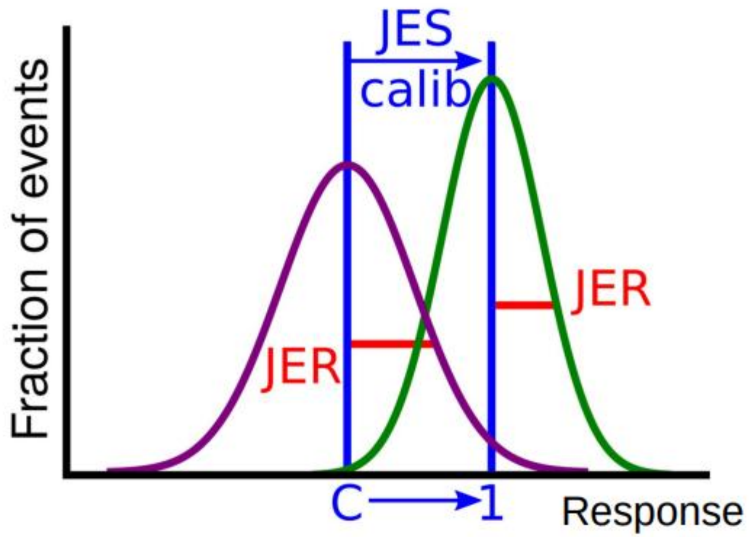

Transformer networks for constituent-based b-jet calibration with the ATLAS detector

ATL-PHYS-PUB-2024-015 & JETM-2026-02

B-jets

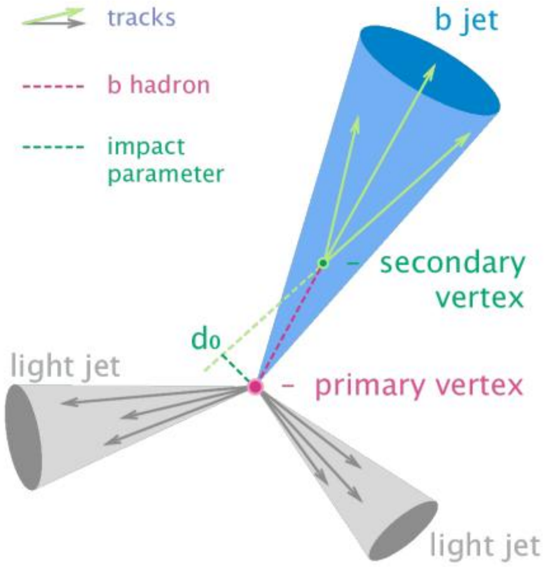

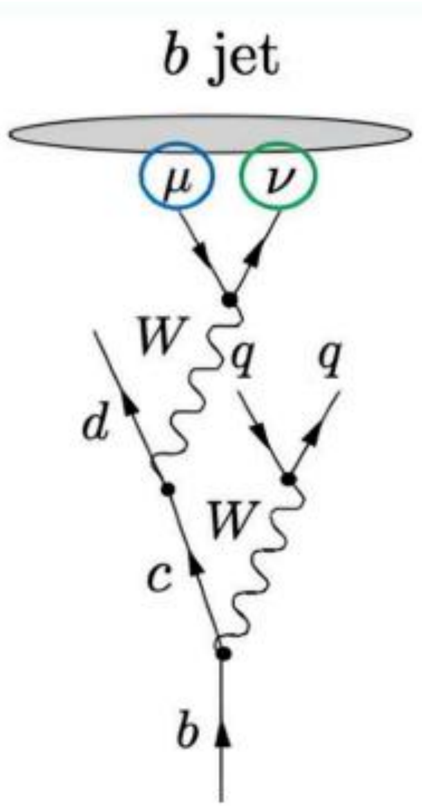

- ATLAS nominal jet calibrations are derived from light quark and gluon jets.
- b-jets have a distinct signature:
  - Secondary vertex (displaced decay)
  - Larger b-quark mass
  - Semi-leptonic decays (substantial branching fraction)
- Current corrections:
  - μ-in-jet: recovers muon p_T lost to semi-leptonic decay
  - PtReco: simple scale factor accounting for neutrino losses (derived in p_T bins)

Transformer architecture

Model architecture based on SALT flavour-tagging models

Small-R: explored the semi-leptonic b-hadrons by adding lepton information to the input features and modifies the truth definition to account for the neutrinos and muons

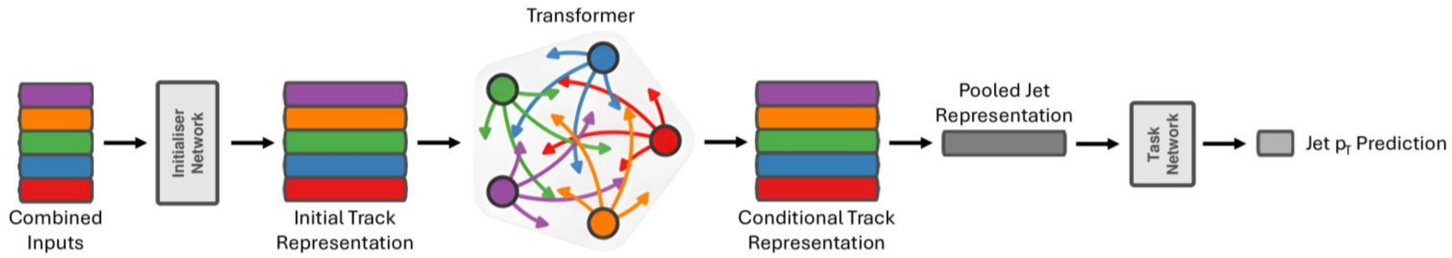

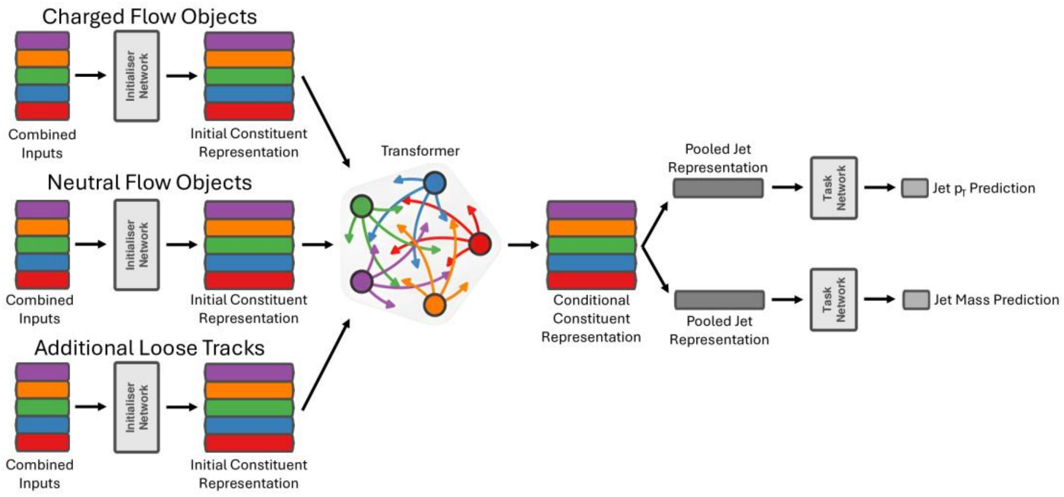

Large-R: Regresses on jet mass as well. Capture all activity within the jet by using both charged and neutral constituents along with additional tracks in the jet that were not included in the clustering.

Small-R performance

- Compare nominal jet calibration with the calibration achieved by applying the transformer-based calibration on top of it
- Study the NN performance w.r.t N_μ
  - Proxy for B-decay channel

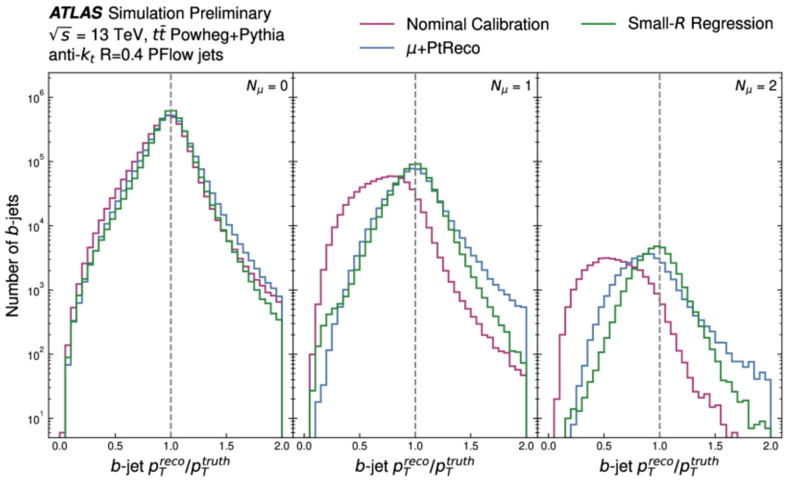

- The new calibration shows the response distributions closer to unity compared to the nominal calibration
  - The relative resolution also improves considerably, up to ≈ 30% improvement
  - Compared to only 20% for $\mu +$ PtReco

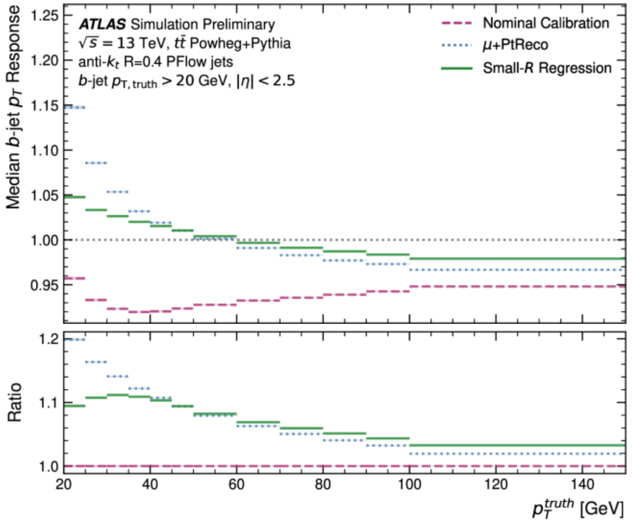

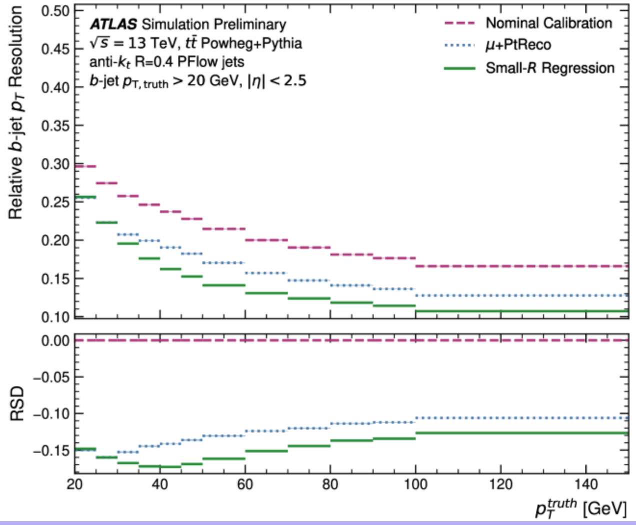

Large-R performance

- Two models were trained:
  - bJR10v00/01: No soft muon information
- Evaluate looking at SM resonances (Z,H,top)
  - Apparent sharpening for the Z/H mass peaks compared to the nominal calibration
  - No mass sculpting from the QCD background
- Overall median response approaches a flat distribution around unity for bJR10v01

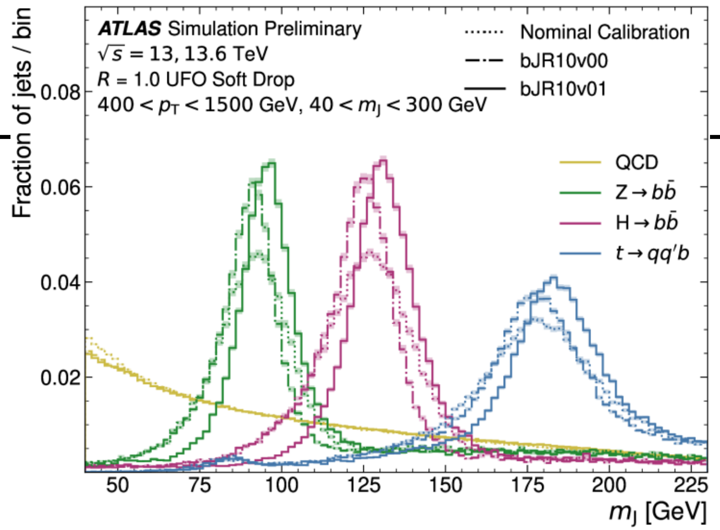

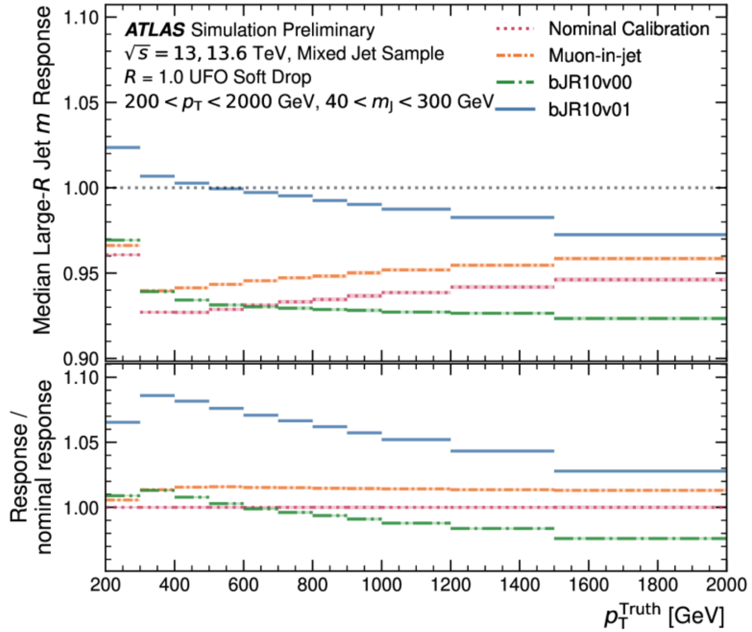

Simultaneous energy and mass calibration of large-radius jets with the ATLAS detector using a deep neural network

JETM-2023-02

η-Annotation

- Difficult for ML models to adapt predictions across η regions
  - Induces η-dependent residual effects
- Solution: **η-annotation**
- Encodes η via 11 Gaussian basis functions $f_i(\eta)$,
  - Provides continuous, localized encoding of jet position
- Improvements are clear in the regions of the detector transition
  - $|\eta| \approx 1.5$ – Barrel-Endcap transition
  - $|\eta| \approx 2.5$ – EM Endcap transition

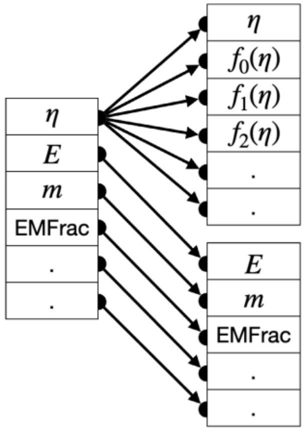

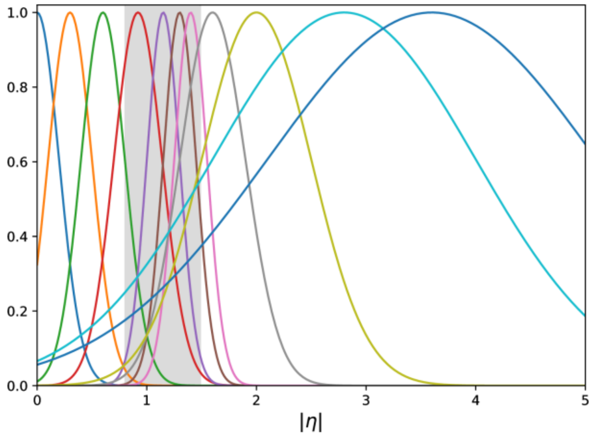

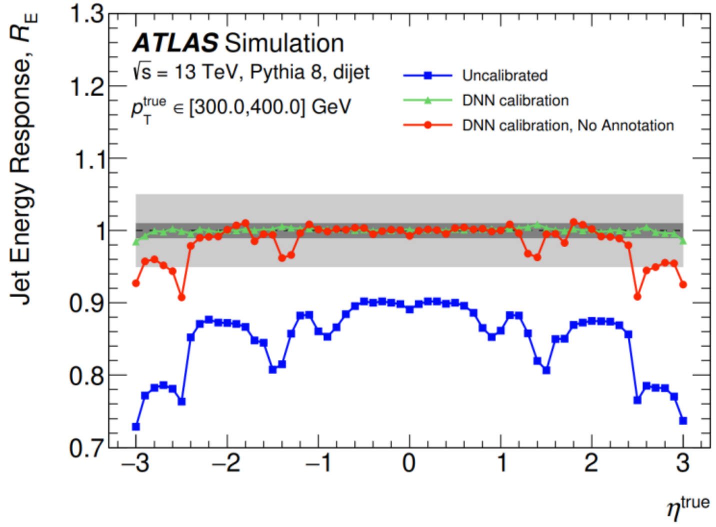

Simultaneous energy and mass calibration

- Utilises a Mixture-density-network (MDN) to calculate mode of the Energy/Mass response
- Input Processing:
  - η-annotation
- Core:
  - Several dense layers common to both energy and mass calibration
- Fork:
  - Individual dense layers to allow for specialisation of each task
- Residual connection:
  - Additional input for the mass calibration to improve the mass prediction
- Output/Predictions:
  - Energy and Mass calibration factors

764k trainable parameters

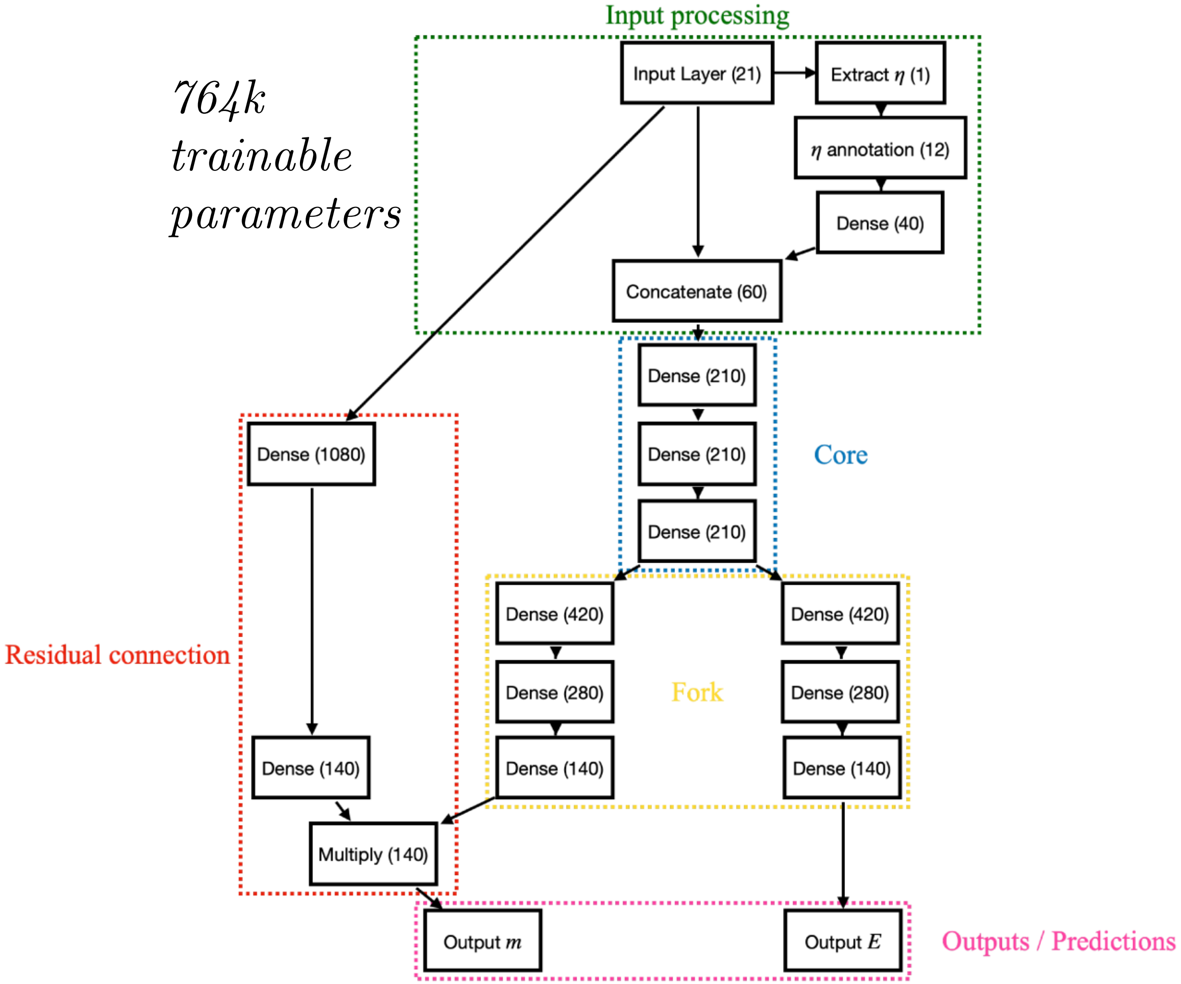

Performance

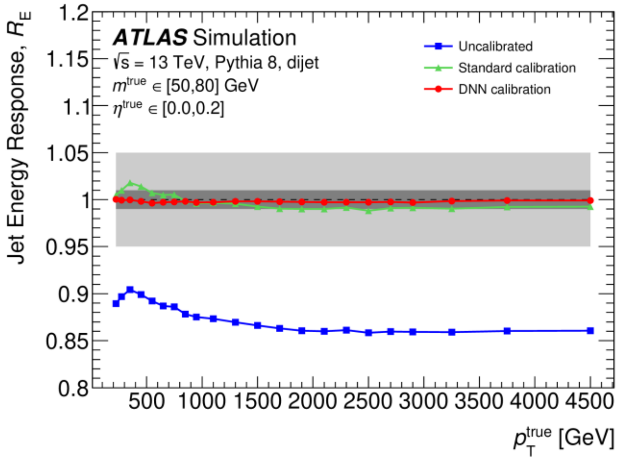

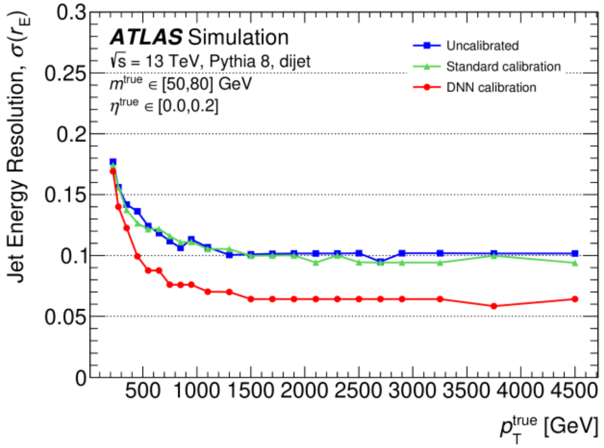

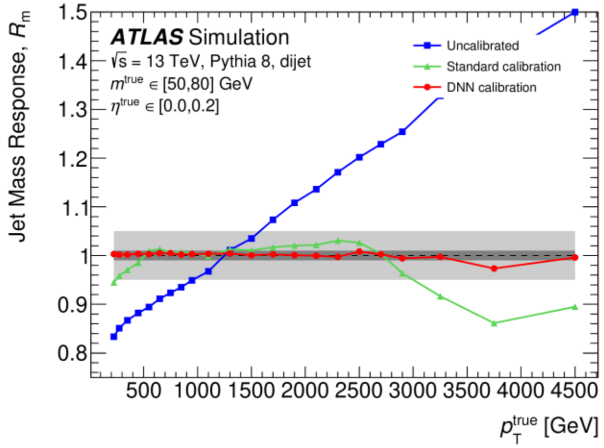

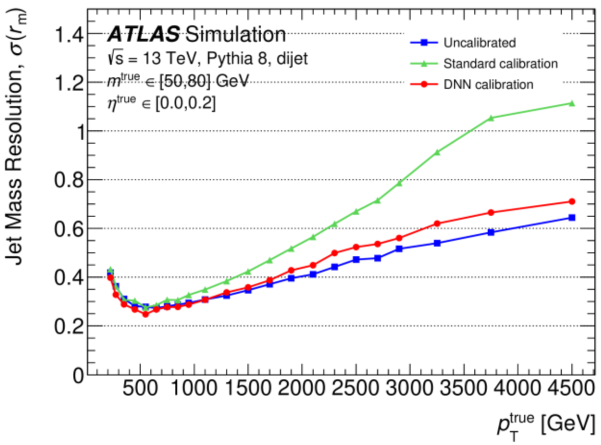

- Excellent response closure for energy
  - Closer to unity than the standard calibration, with an accompanying improvement in the resolution
- Similar closure in the mass response, however, the uncalibrated mas resolution appears better than the calibrated ones.
  - This is a relative quantity while the absolute value of the IQR scales with the central value.

Conclusion

- ML is deeply encoded in the hadronic reconstruction in ATLAS
- State of the art methods are being developed to improve the performance of both constituents and jets:
  - Uncertainty-aware NNs (BNN/HGM) improve topo-cluster calibration over LCW, including at high pile-up
  - Transformer regression improves b-jet resolution by ~30% and sharpens resonance peaks
  - η -annotated DNN calibration corrects detector-transition effects, extending jet energy and mass linearity to the TeV scale
- Continued ML development is essential for the precision and pile-up demands of the HL-LHC era

If theres enough time...

Probabilistic Regression for Jet Energy Calibration: Uncertainty-Aware Machine Learning

[ATL-PHYS-PUB-2026-018]

Probabilistic regression approaches

Targets:

Single-Gaussian:

Single symmetric Normal distribution per jet, with a jet-dependent heteroscedastic mean and variance

$$p(c \mid \vec{x}) = \mathcal{N}\left(c;\, \hat{c}(\vec{x}),\, \sigma_c^2(\vec{x})\right)$$

Mixture-of-Gaussians:

Predicts a weighted sum of K Gaussian components per jet, allowing the conditional response to capture skewed or multi-modal residual structure, with the predictive variance decomposable into within- and between-component terms.

$$p(c \mid \vec{x}) = \sum_{k=0}^{K-1} \pi_k(\vec{x})\, \mathcal{N}\left(c \,\middle|\, \mu_k(\vec{x}),\, \sigma_k^2(\vec{x})\right), \qquad \sum_{k=0}^{K-1} \pi_k(\vec{x}) = 1,$$

Generalised Normal Regression (GNR):

Predicts a single symmetric mode with a learnable shape parameter β that continuously interpolates between Gaussian ($\beta = 2$) and heavy-tailed ($\beta < 2$) behaviour, giving control over tail thickness.

$$p(c \mid \vec{x}) = \frac{\beta(\vec{x})}{2\,\alpha(\vec{x})\,\Gamma(1/\beta(\vec{x}))} \exp\left[-\left(\frac{|c - \hat{c}(\vec{x})|}{\alpha(\vec{x})}\right)^{\beta(\vec{x})}\right]$$

*All three are trained on simulated Run 2 $t\bar{t}$ events and share the same SALT transformer backbone

Performance

- All three probabilistic heads improve the response resolution relative to the nominal in every truth-pT bin and for every flavour.
  - The central response is reduced toward unity most clearly for b-jets at high pT
- The GNR head gives the smallest bin-averaged bias and the most stable calibration behaviour
- Uncertainty can be interpreted as an estimate of the per-jet JER in simulation
  - Reproduces the observed response width to within ~10–15% across the spectrum
  - *simulation only, and no comparison with collision data has been made

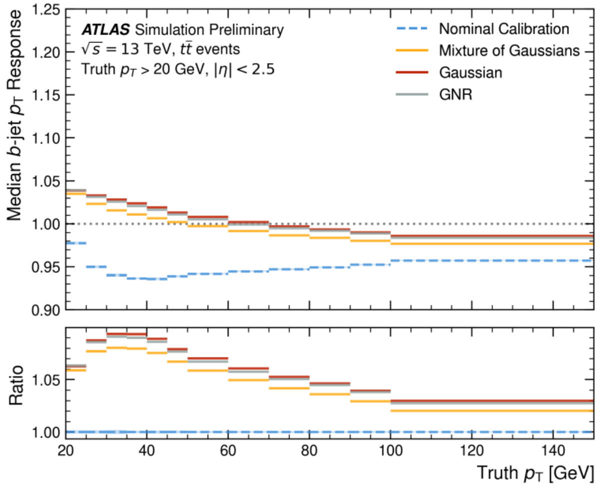

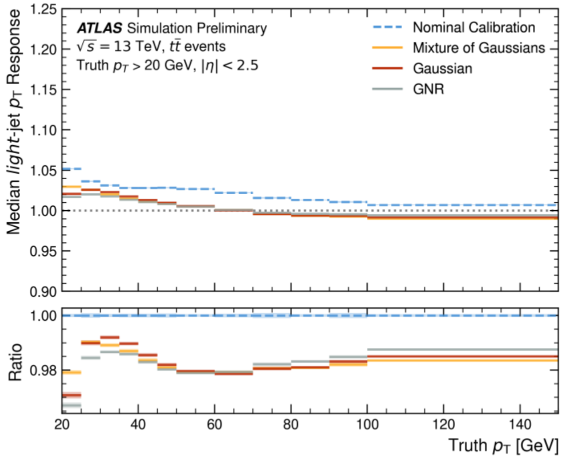

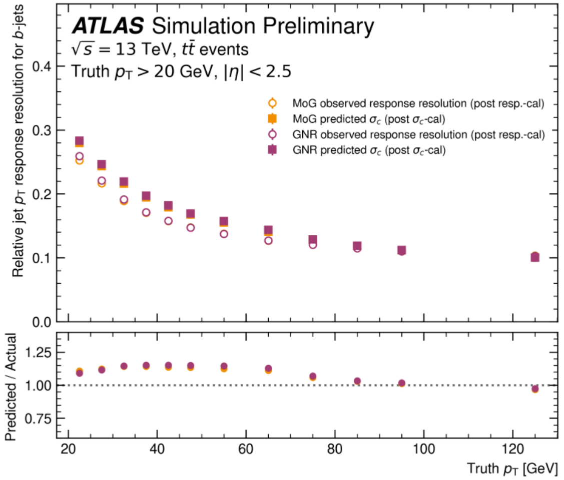

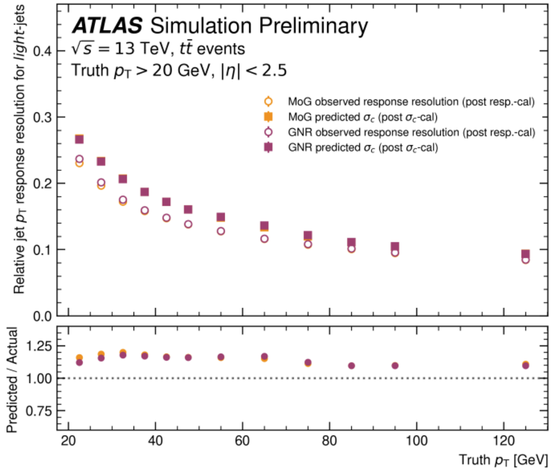

Back-Up Slides

Jet constituent: Topo-clusters

- Topo-clusters are 3D connected-cell objects built from calorimeter cell energies via a topological clustering algorithm
  - Define significance for each cell:
    - Seed Cells: $\zeta_{clus}^{EM} > 4$
    - Neighbour Cells: $\zeta_{clus}^{EM} > 2$
    - Boundary Cells: $\zeta_{clus}^{EM} > 0$

$$\zeta_{\mathrm{cell}} = \frac{E_{\mathrm{cell}}}{\sigma_{\mathrm{noise,cell}}}$$

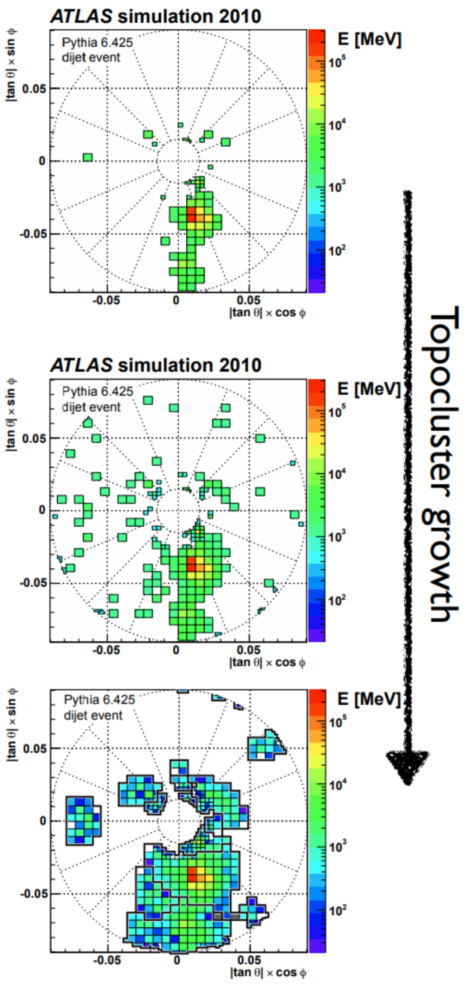

- Cell energies are calibrated at the electromagnetic (EM) scale, correctly measuring EM shower energy
  - Hadronic (HAD) showers deposit energy differently (nuclear breakup, invisible energy), so EM-scale calibration under-measures hadronic energy – motivating further calibration

Topo-cluster calibration

- Usual method: Local Cell Weighting (LCW)
  - Multi-step sequence which has look-up-table corrections
    - w.r.t $\mathcal{P}_{\text{clus}}^{\text{EM/HAD}}$ - likelihood of the topo-cluster being attributed to an EM/HAD-like energy deposit

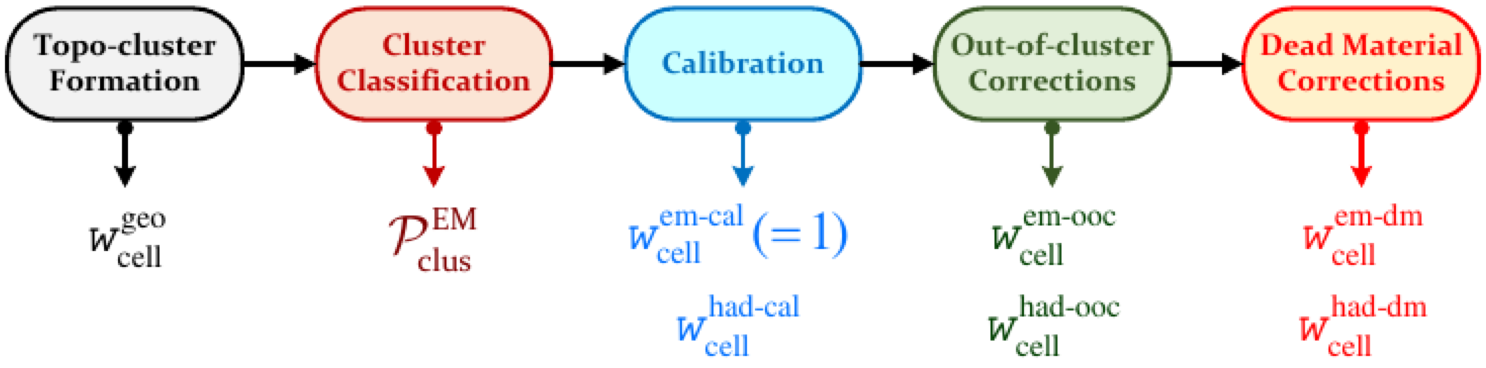

- Calibration factors are extracted from rigid multi-dimensional binned look-up tables and hence bin-edge effects limit performance.

Learned Uncertainties

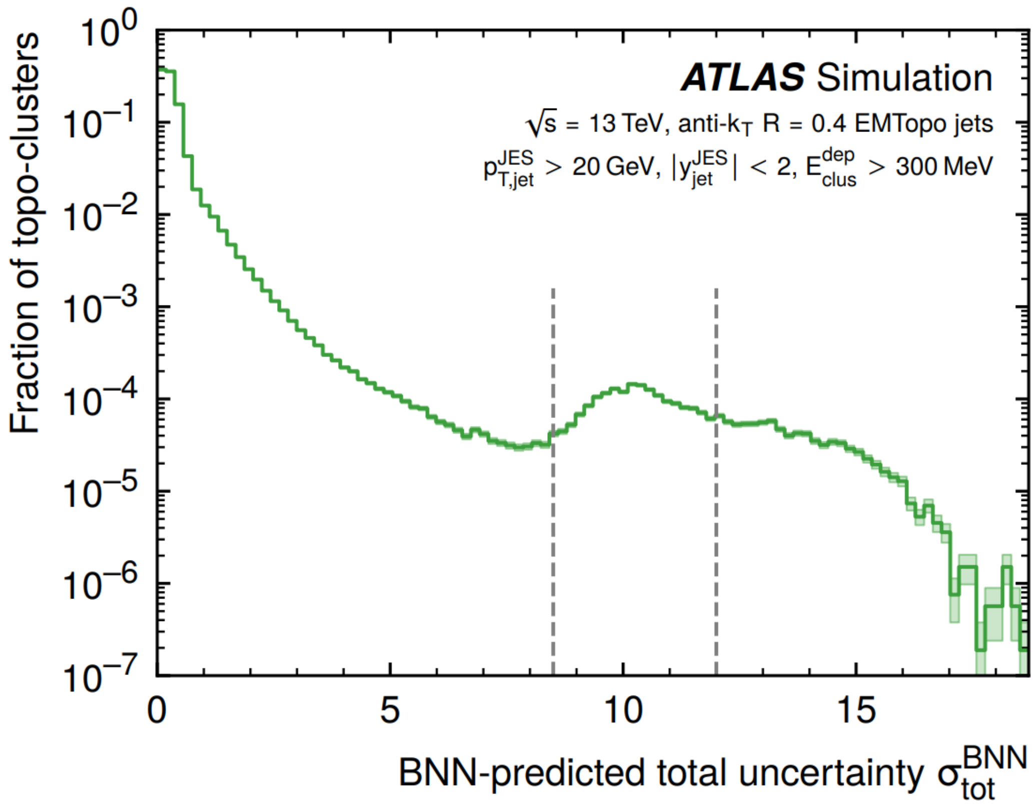

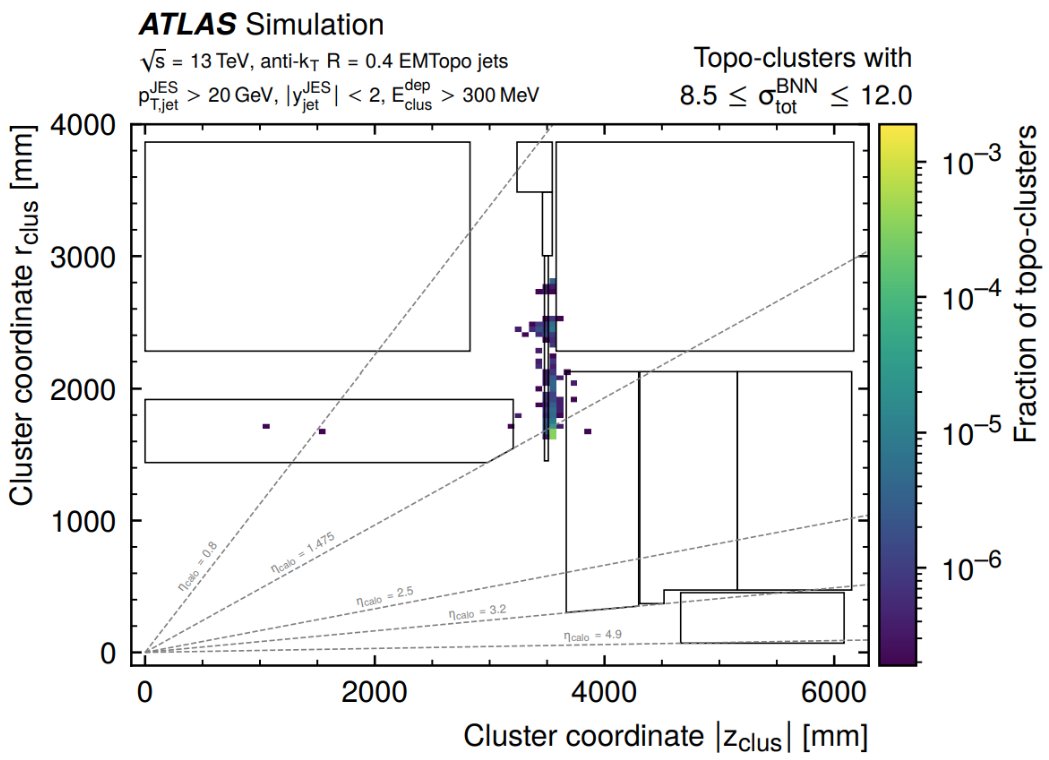

Large R Jet Calibration Chain

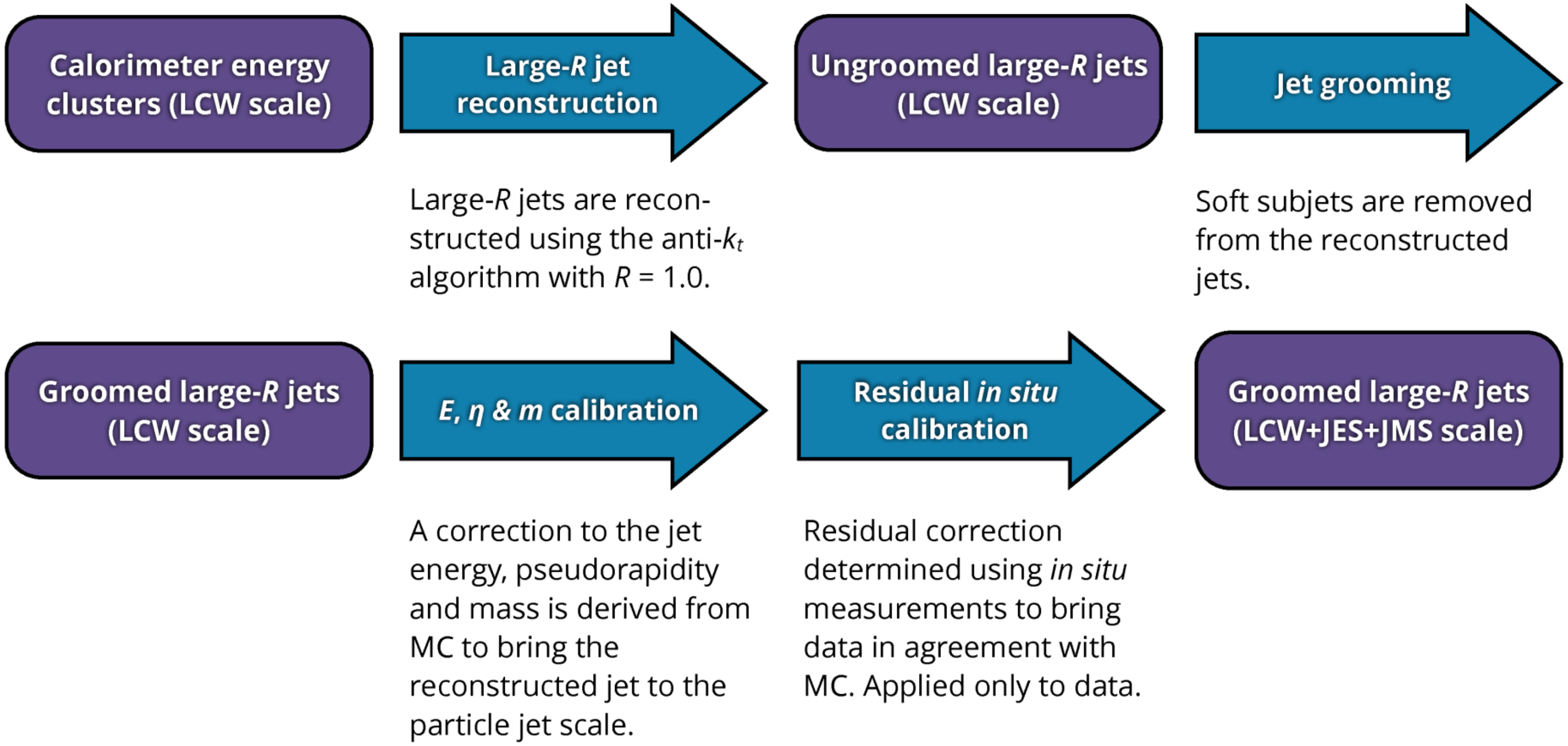

Calorimeter cluster calibration training inputs

Category	Symbol	LCW	Comment
Kinematics	$E^{\mathrm{EM}}_{\mathrm{clus}}$	yes	Signal at the electromagnetic energy scale
	$y^{\mathrm{EM}}_{\mathrm{clus}}$	yes	Rapidity at the electromagnetic energy scale
Signal strength, time structure	$\zeta^{\mathrm{EM}}_{\mathrm{clus}}$	no	Signal significance
	$\mathrm{Var}_{\mathrm{clus}}(t_{\mathrm{cell}})$	no	Variance of t_{cell} distribution
Shower depth, shower shape, compactness	λ_{clus}	yes	Distance of the centre-of-gravity from the calorimeter front face (along principal cluster axis)
	$\lvert\vec{c}_{\mathrm{clus}}\rvert$	no	Distance of the centre-of-gravity from the nominal vertex
	f_{emc}	no	Fraction of energy in the electromagnetic calorimeter
	$\langle\rho_{\mathrm{cell}}\rangle$	yes	Cluster signal density measure
	$\langle\mathfrak{m}^2_{\mathrm{long}}\rangle$	no	Normalised energy dispersion along the principal cluster axis
	$\langle\mathfrak{m}^2_{\mathrm{lat}}\rangle$	no	Normalised energy dispersion perpendicular to the principal cluster axis
	$p_{\mathrm{T}}D$	no	Signal compactness measure (inspired by Ref. [30])
Topology	f_{iso}	yes	Cluster isolation measure
Pile-up	t_{clus}	no	Signal timing
	N_{PV}	no	Number of reconstructed primary vertices
	μ	no	Number of pile-up interactions per bunch crossing

Input features for JETM-2023-02

	Name	Definition
Jet level	E	Energy of the jet in GeV, log E is taken to reduce the spread of its distribution
	m	Mass of the jet in GeV, log m is taken to reduce the spread of its distribution
	η	Jet pseudorapidity
Substructure level	groomMRatio	Mass ratio of groomed to ungroomed jets
	Width	$\sum_i p_{\mathrm{T}i} \Delta R(i, \text{jet}) / (\sum_i p_{\mathrm{T}i})$ where ΔR is the angular distance (sum over the jet constituents)
	Split12,Split23	Splitting scales at the 1st and 2nd exclusive k_T declusterings [34]
	C2, D2	Energy correlation ratios [35, 36]
	τ_{21}, τ_{32}	N-Subjettiness ratios using WTA axis [37, 38]
	Qw	Smallest invariant mass among the proto-jets pairs of the last 3 steps of a k_T reclustering sequence
Detector level	EMFrac	Energy fraction deposited in the electromagnetic calorimeter
	EM3Frac	Energy fraction deposited in the third layer of the electromagnetic calorimeter
	Tile0Frac	Energy fraction deposited in the 1st layer of the hadronic calorimeter
	EffNConsts	$(\sum_i E_i)^2 / (\sum_i E_i^2)$ (sum over the jet constituents)
	NeutralFrac	Energy fraction from neutral constituents
	ChargedPTFrac	p_{T} fraction from charged constituents
	ChargedMFrac	Mass fraction from charged constituents
Event level	μ	Mean number of interactions per bunch crossing
	NPV	Number of primary vertices per event

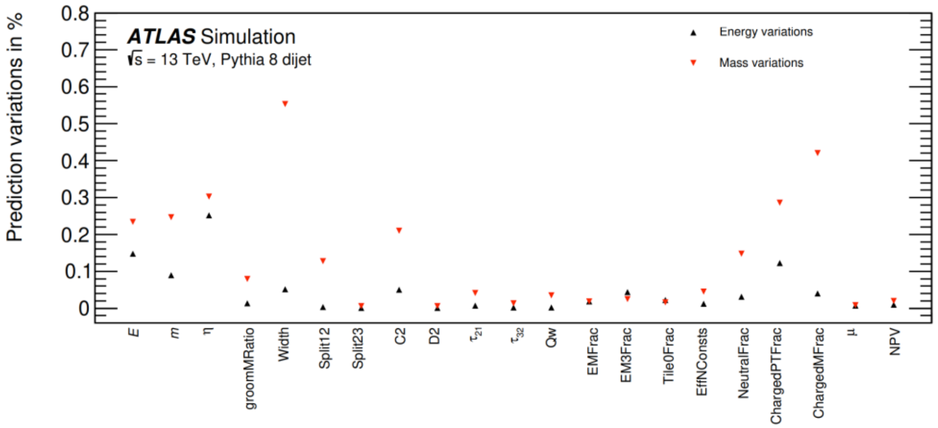

Datasets used for JETM-2023-02

Table 1: Simulated samples used for training and validation

Use	Process type	Generator	Number of jets passing the selections (in millions)
Training, validation	QCD dijet	PYTHIA 8.230	~ 270
Validation	W/Z	PYTHIA 8.230	~ 20
Validation	Top quark	PYTHIA 8.230	~ 15
Validation	Higgs Boson	PYTHIA 8.230	~ 15
Validation	QCD dijet	SHERPA 2.2.5	~ 30

Training used for JETM-2023-02

Table 3: The specific training procedure of the DNN. MDN(A) stands for mixture density network (asymmetric). The loss truncation is indicated in number of standard deviations, σ. When E and m are not mentioned, it means that the energy and mass losses are identical.

Steps	N°	Number of epochs	Batch size	Learning rate	Loss
Initialisation	1	2	15 000	10^{-3}	MDNA
	2	2	25 000	10^{-3}	MDNA
	3	2	35 000	10^{-3}	MDNA truncated (4.0σ)
	4	2	15 000	10^{-3}	MDNA truncated (3.5σ)
Common training	5	6	95000	10^{-3}	MDNA truncated (3.5σ)
	6	6	95 000	10^{-3}	MDNA truncated (3.5σ)
	7	6	125 000	10^{-3}	MDNA truncated (3.2σ)
	8	6	125 000	10^{-3}	MDNA truncated (3.2σ)
	9	10	155 000	5.10^{-4}	MDNA truncated (3.0σ)
	10	15	95 000	10^{-5}	MDNA truncated (E: 3.0σ, m: 2.0σ)
Exclusive mass training	11	50	95 000	10^{-5}	MDN truncated (1.0σ)

Input features for ATL-PHYS-PUB-2024-015

Jet feature	**Description**
p_{T}	Transverse momentum
η	Signed pseudorapidity
m ‡	Jet mass
Track & charged UFO feature	**Description**
q/p	Track charge divided by reconstructed momentum
$\mathrm{d}\eta$	Pseudorapidity of track relative to the jet η
$\mathrm{d}\phi$	Azimuthal angle of the track, relative to the jet ϕ
d_0	Transverse IP: Closest distance from track to beam-line in the transverse plane
$z_0 \sin\theta$	Longitudinal IP: Closest distance from track to PV in the longitudinal plane
$\sigma(q/p)$	Uncertainty on q/p
$\sigma(\theta)$	Uncertainty on track polar angle θ
$\sigma(\phi)$	Uncertainty on track azimuthal angle ϕ
$s(d_0)$	Significance of transverse IP
$s(z_0 \sin\theta)$	Significance of longitudinal IP times the sin of the polar angle
nPixHits	Number of pixel hits
nSCTHits	Number of SCT hits
nIBLHits	Number of IBL hits
nBLHits	Number of B-layer hits
nIBLShared	Number of shared IBL hits
nIBLSplit	Number of split IBL hits
nPixShared	Number of shared pixel hits
nPixSplit	Number of split pixel hits
nSCTShared	Number of shared SCT hits
LeptonID †	Information on if the track was used in lepton reconstruction
Charged & neutral UFO feature	**Description**
$p_{\mathrm{T}}^{\mathrm{Flow}}$ ‡	Transverse momentum of charged flow constituent
E_{Flow} ‡	Energy of charged flow constituent
$\mathrm{d}\eta_{\mathrm{Flow}}$ ‡	Pseudorapidity of track relative to the large-R jet η
$\mathrm{d}\phi_{\mathrm{Flow}}$ ‡	Azimuthal angle of the track, relative to the large-R jet ϕ
$\mathrm{d}r_{\mathrm{Flow}}$ ‡	Angular distance of the track from the large-R jet direction

Soft Muon Input	**Description**
p_{T}	Transverse momentum
η	Signed pseudorapidity
ϕ	Azimuthal angle
dR	Angular distance of the soft muon from the small-R jet axis
q/p	Muon charge divided by the reconstructed momentum
Momentum Balance Significance	Ratio of the difference in momentum measured by the ID and MS to the uncertainty on the energy loss measured by the calorimeters
Scattering Neighbour Significance	Sum of the significances of the angular difference $\Delta\phi$ between pairs of adjacent hits along the track, multiplied by the particle charge
$p_{\mathrm{T}}^{\mathrm{rel}}$	Orthogonal projection of the muon p_{T} onto the jet axis
d_0	Transverse IP: Closest distance from track to beam-line in the transverse plane
z_0	Longitudinal IP: Closest distance from track to PV in the longitudinal plane
$\sigma(d_0)$	Uncertainty on measurement of transverse IP
$\sigma(z_0)$	Uncertainty on measurement of longitudinal IP
$d_0/\sigma(d_0)$	Significance of transverse IP
$z_0/\sigma(z_0)$	Significance of longitudinal IP
Soft Electron Input	**Description**
$p_{\mathrm{T}}^{\mathrm{r}}$	Relative p_{T} of the electron with respect to the jet
dR	Angular separation between electron and jet axis
$p_{\mathrm{T}}^{\mathrm{iso}}$	Isolation variable
$\lvert\eta\rvert$	Absolute value of pseudorapidity
$s(d_0)$	Transverse IP: Closest distance from track to beam-line in the transverse plane
$z(d_0)$	Longitudinal IP: Closest distance from track to PV in the longitudinal plane
$s(d_0/\sigma_{d_0})$	Significance of the transverse IP
$\Delta\phi^{\mathrm{res}}$	The azimuthal angle difference $\Delta\phi$ between the cluster position in the middle layer and the track.
E/p	Ratio of the cluster energy to the track momentum
R_{had}	Ratio of E_{T} in the hadronic calorimeter to E_{T} of the EM cluster
R_{had1}	Ratio of transverse energy E_{T} in the first layer of the hadronic calorimeter to E_{T} of the EM cluster
E_{ratio}	Ratio of the energy difference between the largest and second-largest energy deposits in the cluster over the sum of these energies
$w_{\eta 2}$	Lateral shower width
R_{η}	Ratio of the energy in 3×7 cells over the energy in 7×7 cells centered at the electron cluster position
f_1	Ratio of the energy in the strip layer to the total energy in the EM accordion calorimeter
f_3	Ratio of the energy in the back layer to the total energy in the EM accordion calorimeter
p_{HF}	Probability of being from heavy flavour decay

Datasets used for ATL-PHYS-PUB-2024-015

- Small R

Table 1: Details of the simulation samples used for training and evaluating the small-R jet calibration algorithm. $\ell = e, \mu, \tau$. † Enriched in b-jets.

Process	Generator	Parton shower	PDF set
Training, validation and test samples			
$pp \to t\bar{t}$ fully/semileptonic	POWHEG [29–31]	PYTHIA 8.230 [23] with A14 [32]	NNPDF3.0NLO [24]
$pp \to Z(\mu\mu)$+jets†	MADGRAPH5_AMC@NLO [33] + FXFX [34]	PYTHIA 8.245 with A14	NNPDF3.0NLO
Evaluation samples			
$pp \to Z(\ell\ell)H(b\bar{b})$	POWHEG BOX v2 [29–31] + MINLO [35–37]	PYTHIA 8.230 with AZNLO [38]	NNPDF3.0NLO
$pp \to Z(\ell\ell)Z(b\bar{b})$	SHERPA [27]	SHERPA 2.2.11	NNPDF3.0NNLO

Large R

Table 2: Details of the simulation samples used for training and evaluating the large-R jet calibration algorithm. $\ell = e, \mu$. † QCD jets refer to multijet jet production with heavy-flavour hadron content determined from quantum chromodynamics. ‡ The multijet ($b\bar{b}$) sample provides QCD jets with two b-hadrons, QCD ($b\bar{b}$), as described in the text.

Jet type	Process	Event generator and tune	PDF set
Training, validation and test samples			
$H(b\bar{b})$	$q\bar{q} \to ZH, Z \to \mu^+\mu^-$	PYTHIA 8.306 [23] with A14 [32]	NNPDF3.0NLO [24]
$H(c\bar{c})$	$q\bar{q} \to ZH, Z \to \mu^+\mu^-$	PYTHIA 8.306 with A14	NNPDF3.0NLO
QCD †	Multijet	PYTHIA 8.235 with A14	NNPDF2.3LO
QCD ($b\bar{b}$) ‡	Multijet ($b\bar{b}$), $N_{\text{jet}} \geq 4$, $N_{b-\text{jet}} \geq 2$	PYTHIA 8.235 with A14	NNPDF2.3LO
Evaluation samples			
$H(b\bar{b})$	$q\bar{q}/gg \to ZH$, $Z \to \ell\bar{\ell}/\nu\bar{\nu}/q\bar{q}$	POWHEG v2 +PYTHIA 8.212 [30] with AZNLO [38]	NNPDF3.0NLO
Top	$Z' \to t\bar{t}$	PYTHIA 8.235 with A14	NNPDF2.3LO
$Z(b\bar{b})$	$Z \to b\bar{b}$	SHERPA 2.2.11 [27]	NNPDF3.0NNLO
QCD †	Multijet	PYTHIA 8.235 with A14	NNPDF2.3LO

Full list of papers

- JETM-2026-04: *Calibration and pileup tagging of calorimeter clusters with Machine Learning*
- JETM-2024-01: *Cluster calibration with ML techniques*
- JETM-2026-02: *Large-R jet regression MC and in-situ performance*
- ATL-PHYS-PUB-2024-015: *b-jet MC calibration with transformer networks*
- JETM-2023-02: *Simultaneous energy and mass calibration of large-radius jets with the ATLAS detector using a deep neural network*
- ATL-PHYS-PUB-2026-018: *Probabilistic Regression for Jet Energy Calibration: Uncertainty-Aware Machine Learning*